Shielding and amplification of non-axisymmetric divertor heat flux by plasma response to applied 3-D fields in NSTX and KSTAR

J-W. Ahn[1], K. Kim[2], A.R. Briesemeister[1], G. Canal[3], J.M. Canik[1], T.K. Gray[1], Y. In[4], Y.M. Jeon[4], C.S. Kang[4], J. Kim[4], W.H. Ko[4], H.H. Lee[4], A. Loarte[5], J.D. Lore[1], R. Maingi[6], A.G. McLean[7], J.-K. Park[6], O. Schmitz[8], F. Scotti[7], and S.W. Yoon[4]

[1]Oak Ridge National Laboratory, Oak Ridge, TN 37831, USA

[2]Korea Advanced Institute of Science and Technology, Daejon, South Korea

[3]General Atomics, P.O. Box 85608, San Diego, CA 92186, USA

[4]National Fusion Research Institute, Daejon, South Korea

[5]ITER Organization, Cadarache, France

[6]Princeton Plasma Physics Laboratory, Princeton, NJ 08543, USA

[7]Lawrence Livermore National Laboratory, Livermore, CA 94551, USA

[8]University of Wisconsin – Madison, Madison, WI 53706, USA

E-mail: jahn@pppl.gov

Abstract. Understanding of underlying physics processes that determine non-axisymmetric divertor footprints is crucial for ITER's long pulse operation scenario in the presence of 3-D fields, as they will cause asymmetric erosion and re-deposition of divertor material. It has been recently found that plasma response plays a key role in the formation of 3-D lobe structure and divertor footprints by the applied 3-D fields in NSTX and KSTAR. Work in NSTX showed that ideal plasma response from the IPEC modeling can significantly shield or amplify vacuum footprints from field line tracing. Comparison of footprint measurements by visible and IR cameras to that from the field line tracing reveals that n=1 magnetic perturbations are significantly amplified while n=3 perturbations are shielded. The mechanism of amplification and shielding is determined by the competition between shielding of resonant components and excitation of non-resonant components of applied 3-D fields, demonstrated in the poloidal field spectrum when including plasma response in the modeling. Connection length (L_c) profile from the IPEC modeling for n=1 case shows that L_c rapidly begins to decrease in a significantly deeper region, Ψ_N~0.75, compared to the vacuum case where it only drops near the very plasma edge (Ψ_N~0.97), corresponding to a dramatic amplification of vacuum footprint splitting. However, for the case of n=3 in NSTX, applied 3-D fields are primarily shielded by plasma response; the shielding effect of resonant fields is greater than the amplification effect of non-resonant fields. Shielding and amplification of applied 3-D fields have been also observed in KSTAR by IPEC plasma response modeling. A full phase scan ($\Delta\phi$=0 – 360^o) was conducted for n=1 perturbations, while two distinctive phases, 90^o (resonant) and 0^o (non-resonant), were closely examined for n=2 perturbations. As in NSTX, non-resonant components of applied fields are amplified due to kink excitation while resonant components are strongly shielded, which produces net amplification (shielding) effect of applied fields that strengthens (weakens) footprint splitting for n=1 (n=2), depending on which action is more dominant. Radial location of lobes in the measured heat flux profile shows better agreement with that from the field line tracing when plasma response is included in the modeling.

1. Introduction

The use of 3-D magnetic perturbations for various physics purposes such as ELM suppression/mitigation and NTV control is becoming increasingly common. However, non-axisymmetric divertor flux footprints induced by intrinsic and applied 3-D fields are of concern for future machines such as ITER as they lead to non-axisymmetric heat and particle flux and therefore asymmetric erosion pattern at the divertor surface. Elevated erosion level in specific toroidal and radial locations can raise the risk of tile damage and pose higher maintenance cost. Therefore, improved understanding of how 3-D fields produce non-axisymmetric divertor footprints is necessary. Recently, work on several machines including NSTX [1,2,3,4], KSTAR [5], DIII-D [6,7], and ITER [8] showed that plasma response can play an important role in shielding or amplifying externally applied 3-D fields to form very different separatrix splitting pattern from that of vacuum modeling. It is revealed that several factors, such as toroidal mode number (n) of the applied 3-D fields, q95, and the configuration of applied fields, affect the interaction of plasma with 3-D fields. In this manuscript, we present data from NSTX (mid-plane coils only, up to n=3) and KSTAR (top, middle, and bottom row of coils, up to n=2) and report the role of resonant and non-resonant components of 3-D fields in the shielding and amplification of applied fields. Divertor footprints data for NSTX are both from IR (heat flux) and visible (particle flux) camera, but for KSTAR it is primarily from the IR measurement.

2. Effect of 3-D fields on divertor footprints in NSTX

The spherical tokamak geometry of NSTX enables measurement of divertor footprints with almost full toroidal and radial coverage of lower divertor plates, by the use of high-speed visible camera [9]. This data is compared to the IR data [10], which covers narrower region of lower divertor but with higher spatial resolution.

2.1. n=1 application

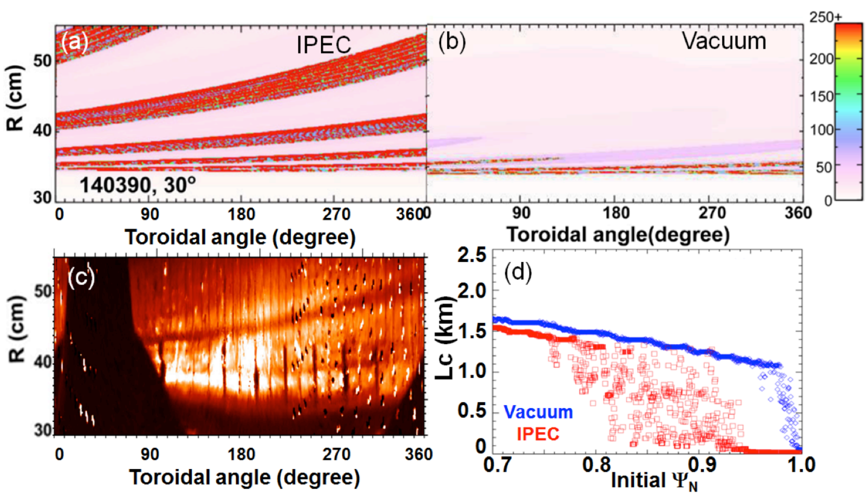

Figure 1 Divertor footprints in the presence of applied n=1 magnetic perturbations in NSTX. (a) and (b) are contour plot of connection lengths from field line tracing with and without ideal plasma response, respectively. Plot (c) is the experimentally observed footprint from a wide angle visible camera. Plot (d) shows the profile of connection length for the vacuum (blue) and ideal plasma response (red) case.

Work in NSTX showed [3,4] that ideal plasma response from IPEC [11] can significantly shield or amplify vacuum footprints from field line tracing. The spherical tokamak geometry of NSTX enables measurement of divertor footprints with almost full toroidal and radial coverage of lower divertor plates. Figure 1 shows footprints with n=1 magnetic perturbations in NSTX. Experimentally observed footprint by a wide angle visible camera is illustrated in figure 1(c). Connection length (L_c) profile for the case of vacuum approximation (blue, figure 1(d)) shows that L_c rapidly decreases only at the very plasma edge (Ψ_N~0.97). This corresponds to the very weak vacuum footprint splitting shown in figure 1(b). However, ideal plasma response dramatically amplifies modeled splitting, see figure 1(a), and this produces a better agreement with the camera image demonstrated in figure 1(c). Accordingly, the L_c profile begins to decrease (red, figure 1(d)), in a significantly deeper region, Ψ_N~0.75, which is a consequence of strong amplification of applied n=1 fields. Figure 2 shows the poloidal spectrum of applied 3-D fields with and without plasma response included in the calculation. It is seen that vacuum calculation produces very weak field

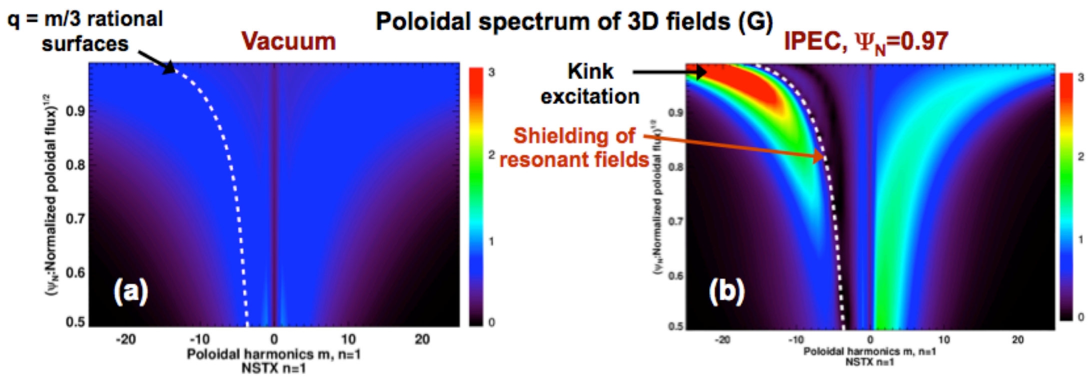

Figure 2 Calculated poloidal spectrum of applied 3-D fields for n=1 in NSTX. Plot (a) is for the case of external fields only, and (b) is for the case of ideal plasma response from IPEC. The simulation boundary for IPEC calculation is Ψ_N~0.97.

spectrum, which is consistent with the weak strike point splitting shown in figure 1(b). As shown in figure 1, the ideal plasma response strongly amplifies non-resonant components of the fields, the so-called kink mode excitation [12], signified by the amplified signal for higher m (< -10) in the edge region ($\Psi_N > 0.9$) and this is directly related to the strong amplification of footprint splitting in figure 1(a). While resonant components (those along the white dashed line) are all shielded off, this amplification of non-resonant components provide strong net effect of enhancing divertor striations as seen in figure 1(c).

2.2. n=3 application

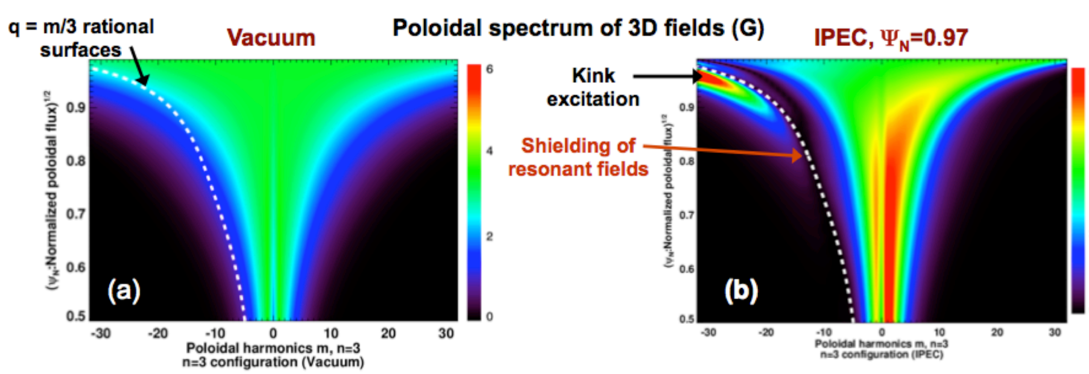

Figure 3 Calculated poloidal spectrum of applied 3-D fields for n=3 in NSTX. Plot (a) is for the case of external fields only, and (b) is for the case of ideal plasma response from IPEC. The simulation boundary for IPEC calculation is Ψ_N~0.97.

Contrary to the case of n=1 application, n=3 fields are primarily shielded by ideal plasma response. Figure 3 shows the calculated poloidal spectrum for the vacuum and ideal plasma response case. It is seen that resonant components are strongly shielded as was in n=1 case, however the amplification of non-resonant components are much smaller than in n=1; the net effect is that shielding of resonant fields is greater than the amplification of non-resonant fields, leading to overall shrink of striations compared to the vacuum case. It is noted, however, that the envelope of striations from the vacuum modeling is well preserved even with the shrinking by plasma response, and the measured heat and particle flux splitting agrees quite well with with vacuum modeling [3,4].

3. Role of resonant and non-resonant fields in divertor heat flux striations in KSTAR

KSTAR is the only machine in operation with the mid-plane 3-D coils along with top and bottom coils. This enables to provide highly aligned pitch of applied 3-D fields, and thus KSTAR is an excellent test-bed to examine the role of resonant and non-resonant components of applied 3-D fields.

3.1. n=1 application

A full phase shift scan ($\Delta\phi$=0 – 360^o) was conducted for n=1 perturbations in KSTAR using upper and middle row of coils. Measured heat flux splitting shows clear phase dependence, with increased splitting and peak heat flux (q_{peak}) for more resonant phase (~90 – 180^o). Figure 4(a) shows average normal field at the plasma boundary both for vacuum and ideal plasma response case, calculated by IPEC, as a function of phase shift angle. This data clearly shows that applied fields are shielded (i.e. plasma response case is smaller than the vacuum) for -40 – +60^o, while they are amplified for 60 – 320^o. Figures 4(b) through 4(d) are measured heat flux profile at the divertor surface for three phase shift angle values, i.e. 0^o, 60^o, and 150^o. It is demonstrated that peak heat flux and striations are strongly affected by the phase angle. As the plasma response moves from shielding (0^o) toward amplification (150^o), both q_{peak} and striations become stronger. Overall, a general trend of net shielding for non-resonant $\Delta\phi$, with weaker strike point splitting, is observed and it moves toward amplification, with splitting becoming stronger, when $\Delta\phi$ becomes more resonant. Poloidal spectra for 0^o (non-resonant) and 150^o (resonant) in figure 5 also exhibits similar trend shown in NSTX as in figures 2 and 3, that competition between shielding of resonant components and amplification of non-resonant components determines the end result of net effect of plasma response. The strong kink excitation for 150^o wins over the shielding effect to produce amplification of applied fields as shown in figure 4(a).

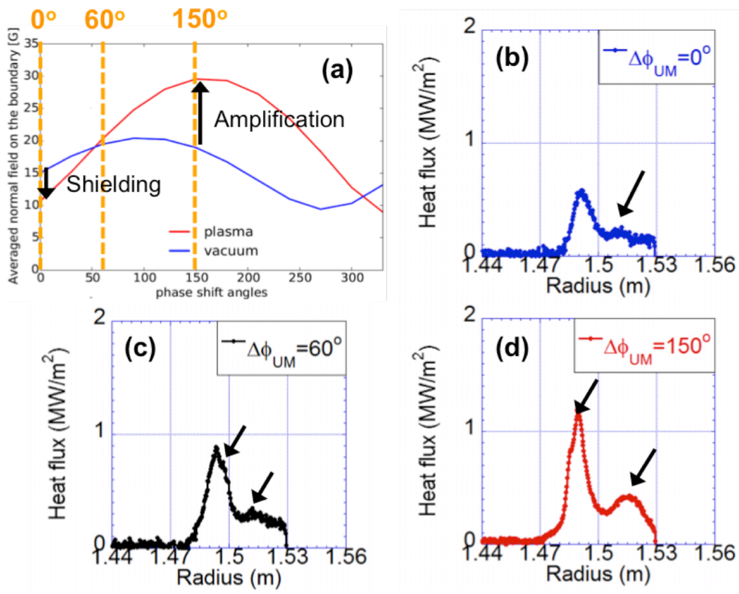

Figure 4 (a) Calculated edge normal field for vacuum (blue) and ideal plasma response (red) cases as a function of phase shift angle ($\Delta\phi$) between upper and mid-plane coils in KSTAR, for a phase shift scan of n=1 perturbation, (b) Measured heat flux profile for $\Delta\phi$=0^o, (c) $\Delta\phi$=60^o, and (d) $\Delta\phi$=150^o. Arrows indicate striations induced to the axisymmetric profile by the applied 3-D fields.

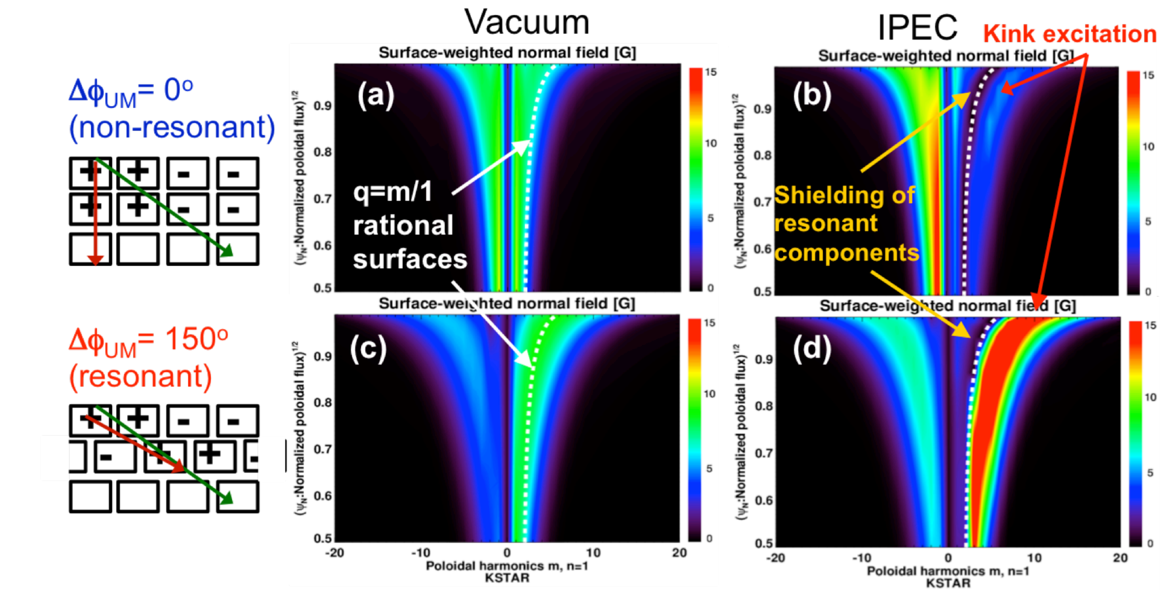

Figure 5 Calculated poloidal spectrum of applied 3-D fields for 0° and 150° of phase shift for n=1 perturbations (top and middle row of coils) in KSTAR. The green arrow in the cartoons in the left indicates equilibrium pitch and the red arrow shows direction of applied fields. Plot (a) and (c) is for the case of external fields only for 0° and 150°, respectively, and (b) and (d) is for the case of ideal plasma response from IPEC.

3.2. n=2 application

AC waveforms were used to produce time varying spectrum of 3-D fields that continuously changed alignment with equilibrium pitch. However, there are only four toroidal segments of coils and this does not allow for continuous scan of phase shift between coil rows for n=2 perturbations. Figure 6 shows time trace of various parameters taken during this experiment. Two distinctive phases were closely examined for n=2 perturbations in this work; resonant (90° phase) and non-resonant (0° phase) configurations. It was revealed that deep penetration of applied n=2 fields is inhibited by the shielding effect of resonant components even with kink excitation of non-resonant components in both phases. Figure 7 shows poloidal spectrum of n=2 fields with 90° phase in KSTAR. As in NSTX, non-resonant components of the

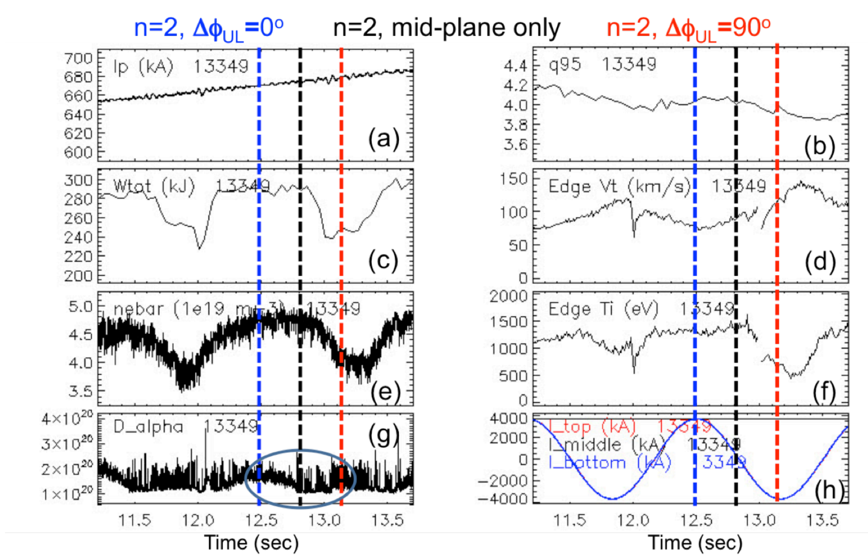

Figure 6 Time trace of various parameters during the n=2 perturbation experiment. Waveform of applied fields is shown in plot (h), from which 0° and 90° of phase shift angle between top and bottom coils is repetitively applied to the plasma. Strong density pump-out as well as reduction of stored energy is observed during the 90° period (red dotted line).

applied n=2 fields are amplified due to kink excitation, see figure 7(b), while resonant components, *i.e.* the field components along the white dashed line in figure 7(a), are strongly shielded. This shielding effect dominates over the amplification effect of non-resonant fields, producing the end result that the applied n=2 fields are significantly screened; see figure 7(c) for comparison of radial profile of total perturbation for the vacuum and IPEC case, which shows net screening of vacuum fields by plasma response. Radial location of lobes in the measured heat flux profile shows better agreement with that from field line tracing when plasma response is taken into account in the calculation. Observed heat flux splitting for 0^o

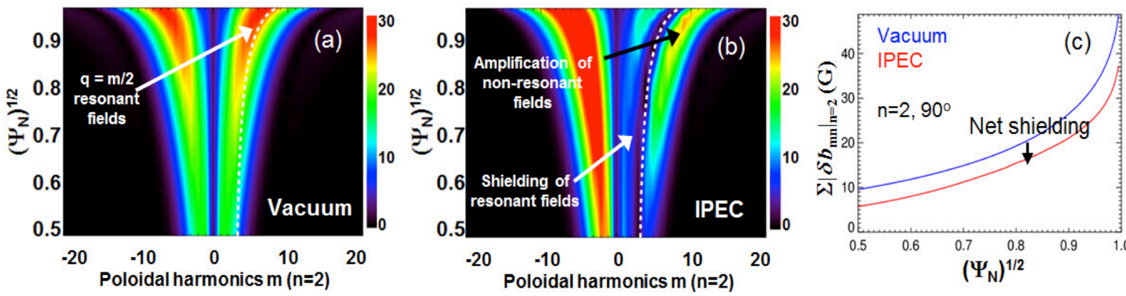

Figure 7 Poloidal spectrum of n=2 fields with 90^o phasing in KSTAR. Plot (a) is for the vacuum case and (b) is for the ideal plasma response case from IPEC. Strong shielding of resonant fields and excitation of non-resonant fields are observed when the plasma response is taken into account. Plot (c) is radial profile of total perturbation, sum over m=[0, 20], for vacuum and IPEC, showing net shielding effect of applied fields by plasma response.

phase is stronger than 90^o. This is consistent with that shielding effect should have been stronger for 90^o due to higher toroidal rotation speed (V_t) as has been observed by CES measurement (see figure 6(d)). Figure 8 shows non-axisymmetric footprints by n=2 perturbations (0^o and 90^o), calculated by field line tracing, as well as comparison to measured heat flux profiles by IR camera. The IR camera is located at the toroidal angle of 45^o and a vertical line is overlaid to indicate its location in the (r, ϕ) plane. Comparing the vacuum and plasma response case, it is seen that agreement for the radial location of striations with measured heat flux profile is noticeably improved when plasma response is included in field line tracing. It is also shown that non-axisymmetric striations become weaker for the plasma response case for both 0^o and 90^o cases. This result is consistent with the net shielding effect for n=2 demonstrated in the poloidal spectrum calculation (see figure 7 for 90^o case).

4. Summary and conclusions

Impact of applied 3-D fields on divertor footprints has been investigated in NSTX and KSTAR. The role of resonant and non-resonant components in forming the strike point splitting and lobe structures was closely examined. Ideal plasma response from IPEC was used to calculate poloidal spectrum of applied 3-D fields as well as in the field line tracing to obtain divertor footprints. Measured divertor footprints from both visible and IR cameras were compared to the calculated footprints in the presence of various configurations of applied 3-D fields. A common feature of ideal plasma response derived from these analyses is that non-resonant components are amplified by kink excitation while resonant ones are shielded. The degree of amplification and shielding varies upon the configuration of 3-D fields as well as the B-field pitch of equilibrium. Competition between these two opposite action of plasma response determines if the externally applied 3-D fields are to be shielded or amplified. In NSTX, due to the lack of top and bottom row of coils, alignment of applied fields to the equilibrium pitch cannot be easily controlled. Nonetheless, we investigated the

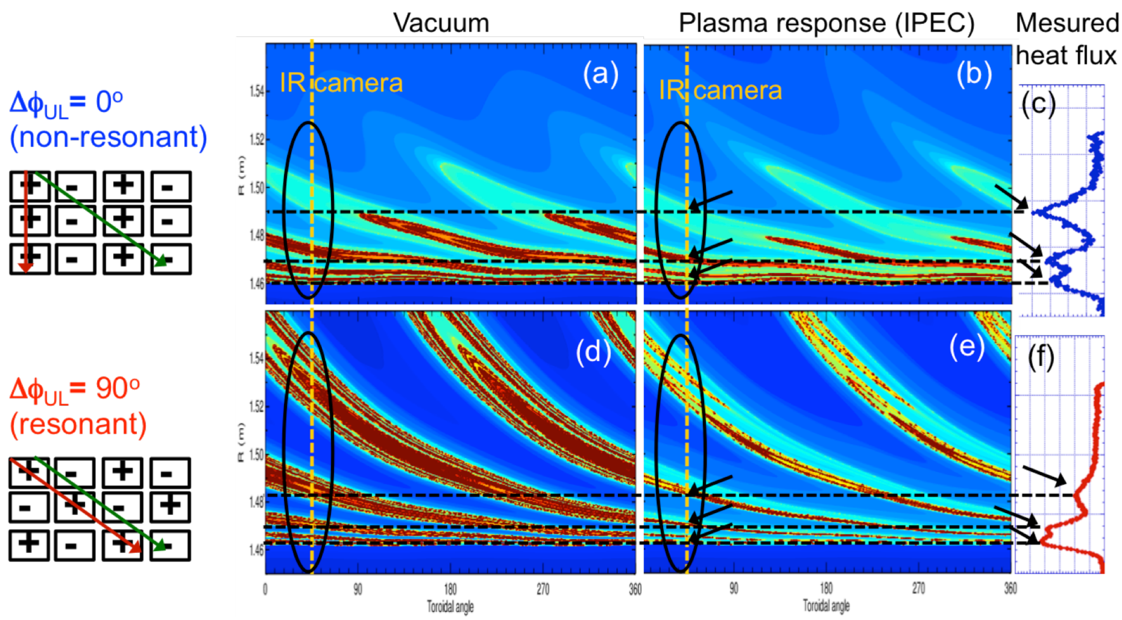

Figure 8 Divertor striation patterns from field line tracing for phase shift angle of 0° and 90° of n=2 perturbations in KSTAR, both for vacuum and ideal plasma response case. The green arrow in the cartoons in the left indicates equilibrium pitch and the red arrow shows direction of applied fields. Plot (c) and (f) are measured heat flux profile for comparison to field line tracing result. Dotted vertical line indicates the toroidal location of IR camera for the heat flux profile in plots (c) and (f). Black arrows are to highlight striations induced by 3-D fields.

case of n=1 and n=3 fields and found that n=1 fields are strongly amplified by the plasma response to enhance divertor striations. However, n=3 fields are primarily shielded by the plasma response and the overall striation pattern is similar to the one from the vacuum modeling. Comparing poloidal spectra for n=1 and n=3 with the plasma response included, it is found that the level of kink amplification for n=1 is dramatically higher than n=3, making the net effect of plasma response strongly toward the enhancement of divertor striations. This result is supported by the measured heat and particle flux profiles.

On the other hand, KSTAR has three rows of coils to apply external 3-D fields. This is very advantageous because of the capability of fine-tuning the pitch alignment as well as continuous variation of phase shift between different rows of coils for n=1, although only two distinct phases (0^o and 90^o) are available for n=2 due to the limited number (=4) of toroidal sector of coils. For n=1 application, it is shown that edge magnetic fields are either shielded or amplified depending on the phase shift between top and middle row of coils. Moving from shielding toward amplification, the peak heat flux and strike point splitting of measured heat flux profiles become stronger, which is consistent with the result of poloidal spectrum calculation and field line tracing. For the n=2 application, both 0^o and 90^o show shielding of applied fields by the plasma response. Divertor footprint striations are much stronger for the resonant case (90^o) in the vacuum calculation, and this trend is maintained even with the inclusion of ideal plasma response in the calculation. Comparison to measured heat flux profiles revealed that field line tracing result with plasma response provides better agreement with the experimental data both for 0^o and 90^o of phase shift.

References

[1] Ahn, J-W., et al., “Modification of divertor heat and particle flux profiles with applied 3-D fields in NSTX H-mode plasmas”, Nucl. Fusion **50** (2010) 045010.

[2] Ahn, J-W., et al., “Study of non-axisymmetric divertor footprints using 2-D IR and visible cameras and a 3-D heat conduction solver in NSTX”, J. Nucl. Mater. **438** (2013) S317

[3] Ahn, J-W., et al., “Characterization of divertor footprints and the pedestal plasmas in the presence of applied n=3 fields for the attached and detached conditions in NSTX”, Plasma Phys. Control. Fusion **56** (2014) 015005.

[4] Kim, K., et al., “Ideal plasma response to vacuum magnetic fields with resonant magnetic perturbations in non-axisymmetric tokamaks”, Plasma Phys. Control. Fusion **57** (2015) 104002.

[5] Ahn, J-W., et al., “Shielding and amplification of non-axisymmetric divertor heat flux by applied 3-D fields in KSTAR”, KSTAR Conference, February 25 – 26, 2016, Daejeon, South Korea

[6] Schmitz, O., et al., “Formation of a three-dimensional plasma boundary after decay of the plasma response to resonant magnetic perturbation fields”, Nucl. Fusion **54** (2014) 012001.

[7] Jakubowski, M.W., et al., “Overview of the results on divertor heat loads in RMP controlled H-mode plasmas on DIII-D”, Nucl. Fusion **49** (2009) 095013.

[8] Schmitz, O., et al., “Three-dimensional modelling of plasma edge transport and divertor fluxes during application of resonant magnetic perturbations on ITER”, Nucl. Fusion **56** (2016) 066008.

[9] Scotti, F., et al., “Full toroidal imaging of non-axisymmetric plasma material interaction in the National Spherical Torus Experiment divertor”, Rev. Sci. Instrum. **83** (2012) 10E532

[10] Ahn, J-W., et al., “High speed infrared camera diagnostic for heat flux measurement in NSTX”, Rev. Sci. Instrum. **81** (2010) 023501

[11] Park, J-K., et al., “Computation of three-dimensional tokamak and spherical torus equilibria”, Phys. Plasmas **14** (2007) 052110

[12] Lanctot, M.J., et al., “Measurement and modelling of three dimensional equilibria in DIII-D”, Phys. Plasmas **18** (2011) 056121